ISSN 1392-3730/eISSN 1822-3605

JOURNAL of CIVIL ENGINEERING and MANAGEMENT

2026
Volume 32
Issue 6
Pages 818–833
https://doi.org/10.3846/jcem.2026.26525

MULTIDISCIPLINARY APPROACH TO THE STRUCTURAL, HYDRAULIC, AND MECHANICAL DESIGN OF A STEEL DECAY VESSEL FOR THE SHIP EXPERIMENT AT CERN

Fabrizio ALOSCHI[1,2]✉, Andrea MIANO[2,3], Antimo FIORILLO[1,2], Oreste FECAROTTA[2,4], Cristiana DI CRISTO[2,4], Giuseppe DEL GIUDICE[2,4], Giovanni DE LELLIS[2,5], Richard JACOBSSON[2], Andrea PROTA[1,2]

[1] *Department of Structures for Engineering and Architecture, University of Naples "Federico II", Via Claudio 21, 80125 Naples, Italy*
[2] *European Organization for Nuclear Research (CERN), Espl. des Particules 1, 1217 Genève, Switzerland*
[3] *Department of Engineering, Telematic University "Pegaso", Centro Direzionale Isola F2, 80143 Naples, Italy*
[4] *Department of Civil, Architectural and Environmental Engineering, University of Naples "Federico II", Via Claudio 21, 80125 Naples, Italy*
[5] *Department of Physics "E. Pancini", University of Naples "Federico II", Via Cintia Building 6, 80126 Naples, Italy*

Article History:
- received 2 July 2025
- accepted 16 January 2026

Abstract. In March 2024, the Search for Hidden Particles (SHiP) experiment and its associated Beam Dump Facility (BDF) were selected for future physics exploitation using the Super Proton Synchrotron (SPS) at CERN. SHiP is a general-purpose, intensity-frontier experiment designed to search for dark matter-related physics. Proposed approximately a decade ago, the SHiP experiment has passed through multiple design stages and optimizations. This study focuses on the structural design of primary subcomponent of SHiP, i.e., "the decay volume", where the experiment seeks decay signatures of new particles. Initial concepts included a reinforced-concrete structure with hollow rectangular cross-sections exceeding 10 m × 5 m, evolving to a 50-m-long conical steel vessel under vacuum, and more recently to a metal-framed helium balloon, which is a textile helium seal supported by steel frames. We present the structural and hydraulic configurations now considered the final reference solutions for decay vessel of the SHiP to highlight the unique engineering challenges of minimizing structural mass, thereby reducing particle interactions and enhancing physics performance. To provide context, the paper first summarizes the collaboration status of SHiP and subsequently reviews the sequence of decay vessel structural options explored since the inception of the project. This historical overview depicts how the decade-long, multidisciplinary effort shaped current design choices. Furthermore, it illustrates how a novel, multidisciplinary, integrated approach guided the design evolution of the decay vessel. In the context of large-scale international collaborations such as SHiP, this paper demonstrates that a coordinated strategy integrating structural, hydraulic, and detector requirements has seldom been applied in similar large experimental facilities. As demonstrated in this study, such an approach proved essential for achieving a configuration that satisfies engineering constraints while preserving the experiment's physics performance goals. The principal outcome of this effort is the proposed final design strategy, which coalesces engineering and physics goals into a unified framework. This methodology ensured that all subsystem interactions were considered concurrently to prevent costly redesigns during project execution. The final design strategy separates the mechanical system of the decay vessel into two key components: (i) a structural steel framework and (ii) non-structural aluminum elements, both integrated with a complex hydraulic system to circulate a specific detection liquid. This division maintains functional and structural efficiency and offers flexibility to adapt to seismic-condition variations throughout the project.

Keywords: SHiP experiment, decay vessel, steel structure, aluminum structure, hydraulic design, CERN.

✉Corresponding author. E-mail: ***fabrizio.aloschi@unina.it***

1. Introduction

The existence of dark matter and the observation of additional phenomena unexplained by the Standard Model of Particles and Fields have prompted physicists to explore the entire phase space extensively and search for new particles as potential solutions to these mysteries. The European Organization for Nuclear Research (CERN) is leading the effort on these searches with accelerator-based technologies. It recently opened a new path toward potential discoveries with the construction of the SPS Beam Dump Facility (BDF). The facility exploits high-intensity proton beams from the SPS accelerator and is specifically designed to carry out the search for long-lived, i.e., very-feebly interacting, particles. The Search for Hidden Particles (SHiP) experiment will operate at the BDF and will perform world-leading searches for new feebly interacting particles (Abbaneo et al., 2025; Ahdida et al., 2022).

The BDF/SHiP facility will operate in the North Area of CERN, as depicted in Figure 1 from Ahdida et al. (2022). Hidden particles are expected to undergo particle decay within the so-called decay volume, which must be surrounded by a liquid scintillator detector layer known as the Surrounding Background Tagger (SBT) to tag particles originating externally. Downstream, a spectrometer will detect the products of these particle decays. In this article, we review the various structural design proposals for this volume and present its associated systems. Over the last decade, these proposals have been discussed and evaluated, highlighting the pros and cons of the different solutions. Numerous design alternatives have been proposed, ranging from a reinforced concrete structure with large hollow rectangular sections to a conical steel vessel operating under vacuum and finally a steel-framed helium balloon that integrates a textile material to contain helium, with aluminum boxes providing structural stability. A decade-long multidisciplinary design effort has generated a significant research challenge in structural engineering. The primary objective throughout this effort was to minimize structural component mass, thereby reducing particle interactions with the structure to enhance detection performance. Ultimately, the goal is to optimize physics outcomes while fully complying with structural code requirements. This objective poses a significant challenge for steel structure optimization (Minh et al., 2024; Svendsen et al., 2023; Truong & Chou, 2023; Venskus et al., 2010) and cost savings (Alshibani et al., 2024; Elmousalami, 2020). Moreover, the challenge intensifies owing to interactions between the structural steel framework and the aluminum system (Georgantzia et al., 2021), especially as seismic conditions, and thus, the seismic demand on the decay vessel, are expected to evolve over the project duration.

To address these challenges, we recall that the behavior of lightweight shells and plate-like structures under complex loading has been extensively studied in existing literature. Early theoretical frameworks, based on the theory of plates and shells (Mittelstedt, 2023), and developments derived from membrane theory of shells (Zingoni, 2017), provide the principles governing thin-walled mechanical system behavior. These thin-walled systems typically withstand applied loads while minimizing material usage. In particular, recent studies have examined optimization under varying or nonlinear loading conditions, including research on integrated load optimization of elastic–plastic axisymmetric plates at shakedown (Venskus et al., 2010). Notably, that study solved a load optimization problem combining von Mises and Tresca yield criteria, demonstrating how structural components could be designed to endure repeated variable loading and avoid progressive plastic deformation. In contexts with seismic and operational variability, such as the SHiP project, updated finite element model (FEM) approaches employing sensitivity analysis in full-scale steel structures (Svendsen et al., 2023) demonstrated that iterative, data-informed structural improvement is essential to achieve sufficient performance under real-world uncertain demands. The SHiP project involves coordinating various interdependent subsystems such as electrical infrastructure, fire safety management, evacuation procedures, and operational variability, which further illustrated these requirements.

The aforementioned works depict a scenario where designing lightweight large-scale structures necessitates combining theoretical modeling, optimization strategies, and structural verification. However, compared with traditional civil and mechanical structures, the decay vessel in this project introduces additional complexities: minimizing mass for physics performance, integrating steel–aluminum components with distinct mechanical behaviors, considering internal pressures resulting from its vacuum configuration, and accommodating evolving seismic demands over the project timeline. As described in this paper, these constraints require careful structural formulation and a coor-

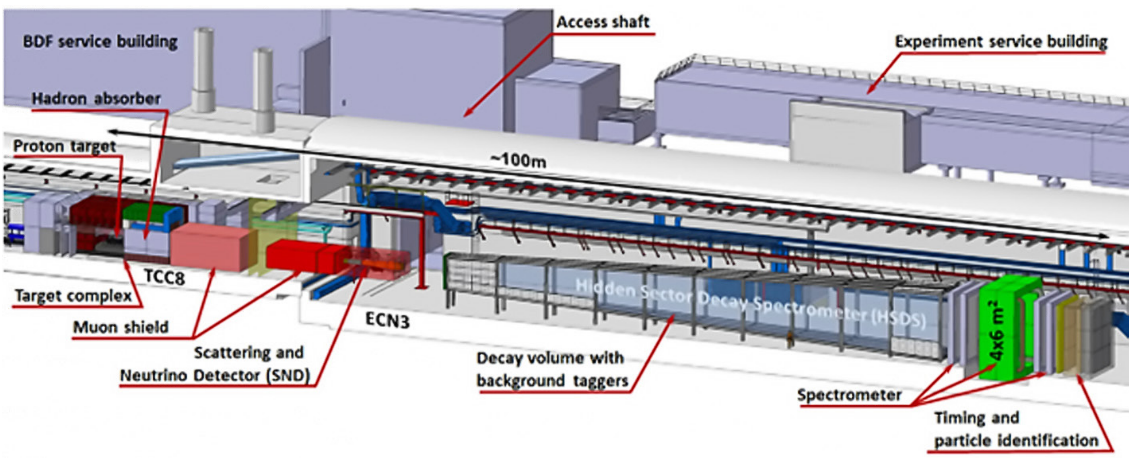

Figure 1. Schematic of beam dump facility and SHiP detector

dinated multidisciplinary design process to adapt to continuously changing operating conditions.

Another design challenge concerns pumping the liquid scintillator used for particle detection into the cavity surrounding the vessel through a hydraulic system. Moreover, rapid emptying of the system is necessary in case of an emergency, such as fire. Considering the liquid scintillator characteristics, this work presents a design solution for the pumping system and hydraulic circuit, along with adequate procedures for filling and emptying.

Filling and emptying are periodically performed in water pipelines for maintenance, cleaning, or repairs (Fuertes-Miquel et al., 2019). When pipelines are rapidly filled, dynamic and sometimes dramatic air–water interactions often occur (Zhou et al., 2018). These air–water interactions, along with their associated pressure and temperature oscillations, have been widely explored in the literature both experimentally (e.g., De Martino et al., 2008; Zhou & Liu, 2013), and numerically (e.g., Zhou et al., 2011, 2018). The filling process begins when a discharge valve is opened, and the liquid column driven by an energy source (tank or pump) starts to fill the system by compressing the entrapped air pocket (Hou et al., 2014; Malekpour et al., 2016; Martins et al., 2017). The emptying process starts when drain valves located at the low points of the system are opened, and water is replaced by airflow (Coronado-Hernández et al., 2018; Fuertes-Miquel et al., 2019; Tijsseling et al., 2016). Filling processes should be executed carefully through slow maneuvers in the operation to produce an adequate expelled airflow rate (Fuertes-Miquel et al., 2019). For water pipelines, a pressure differential of 13.79 kPa and a flow velocity of 0.3 m/s are recommended during this process. Similarly, a controlled emptying process should be performed with a pressure differential of 5 psi (34.5 kPa) and water velocities from 0.3 to 0.6 m/s.

These recommendations derive from circular pipes with water and cannot directly apply to the problem under study, but they have been appropriately adapted to design the hydraulic circuit and the filling/emptying procedures for the specific prototype under consideration. In this application, the fluid is not water but a mixture of linear alkylbenzene (liquid scintillator), which must fill parallelepiped-shaped boxes instead of pipes. Moreover, the design of the hydraulic circuit and the filling/emptying procedures must respect specific constraints imposed by the planned experiment. The first constraint requires performing a filling process that eliminates air from the system, as the presence of air pockets would create problems in particle detection and thus compromise the experiment. The second constraint limits the maximum emptying time, which must be set according to safety requirements. The characteristics of the planned SHiP experiment and of the vessel structure require a dedicated study to devise an appropriate, original solution.

The remainder of this paper is structured as follows. The status of the SHiP Collaboration project is briefly described in Section 2. A comprehensive overview of the initial design solutions specifically proposed at the outset of the SHiP project is presented in Section 3. The design guidelines and the currently accepted structural design details for both vacuum and helium configurations are detailed in Section 4. Thereafter, the design of the pumping system and the filling and emptying procedures are discussed in Section 5, with the conclusions of this study summarized in Section 6.

2. Status of the SHiP collaboration and summary of the project

SHiP is presently composed of 33 participating institutes and 5 associated institutes, spanning 15 countries, along with CERN. In particular, its organizational structure comprises a Collaboration Board (CB), an elected Interim Spokesperson, a Technical Coordinator, a Physics Coordinator, and a team of project conveners approved by the CB. Furthermore, the defined work packages for SHiP are based on foundational designs established over six years of joint research efforts in the Technical Proposal and Comprehensive Design Study (CDS) phases, which focused intensively on optimizing component designs to enhance signal acceptance and overall physics performance. Moreover, all key components of the SHiP facility have been investigated, analyzed, and, in several cases, prototyped. Subsequently, an initial validation of the target system replicated the actual operating conditions of the final target (Lopez Sola et al., 2019), and each SHiP sub-detector has undergone initial prototyping and experimental evaluation. Additionally, larger-scale prototypes have been developed for the liquid scintillator-based technology intended for the Surround Background Tagger (SBT), as introduced later, as well as for the scintillating-bar technology planned for the timing detector. These tests identified the primary technological challenges that must be addressed in the upcoming Technical Design Report (TDR) phase. Based on these findings, all major detector subsystems, including those of the Decay Vessel, underwent conceptual design reviews that defined the scope and direction of work leading to the TDR.

The primary technical challenges faced by SHiP relate to the implementation and cooling of the target system and to the design and operational management of the overall target complex. One promising avenue to enhance physics performance, particularly by reducing decay heat within the decay vessel, involves developing niobium-alloy cladding. To maintain an inert atmosphere in the decay vessel, which mitigates corrosion and minimizes residual gas radioactivation within the target shielding, three options have been considered: helium, nitrogen, or vacuum. These options, as well as the design of the nearby shielding and supporting infrastructure, require comprehensive investigation. In this paper, only the structural designs for the helium and vacuum configurations are detailed, as a nitrogen configuration has not been developed sufficiently to support detailed analysis. Although handling concepts for the target and associated systems are well established, the individual components' complexity and reliance on remote handling techniques demand further detailed engineering, prototyping, and validation efforts to ensure reliable long-term operation. Moving forward, core technological challenges include detailed mechanical development and scaling up to full-size, industrial-scale production.

Figure 2 presents the projected timeline for implementing the Beam Dump Facility (BDF) for SHiP in Experimental Cavern North 3 (ECN3).

The proposed timeline builds upon the experience gained during the CDS phase and is designed to maximize the use of the Super Proton Synchrotron (SPS) in parallel with High Luminosity–Large Hadron Collider (LHC) operations. It considers stringent and complex technical and resource constraints and the construction-phase operating schedule of CERN's beam facilities. The plan relies on the decision to proceed with the high-intensity upgrade of the ECN3 beamline made in the first half of 2023 and on project approval for the TDR phase granted in 2024. Leveraging the three-year CDS study and ongoing BDF R&D efforts, the detailed Technical Design Reports for all BDF components in ECN3 can be completed within two and a half years and within three years for the SHiP detector. This overall timeline aligns with the objective of initiating the initial phased implementation of the BDF during LS3. The LS3 period for the injectors, currently planned for 2026–2027, is a key element in the overall timeline, as it permits the necessary complex upgrades to the beamlines for increased intensity and the required cool-down phase before the expected reactivation of the North Area for Run 4 at CERN. Timely decommissioning of the existing installations in ECN3 can occur in the same period, allowing further infrastructure modifications to commence in the second half of 2027. The overall production of the detector is expected to span three years, and assembly and installation are projected to require an additional two to three years. According to this schedule, a brief commissioning run of the fully functional target complex could occur in the second half of 2030, followed by full operation of the complete detector in 2031.

3. History of the decay vessel structural design: Structural solutions investigated since the beginning of the SHiP collaboration

Beginning in 2013, several decay vessel structural solutions were investigated and presented to the SHiP Collaboration. The design effort intensified in 2016, yielding hybrid reinforced concrete (RC)–steel solutions and fully steel-based configurations. An overview of these approaches follows. Notably, all discussed structural concepts relate exclusively to the vacuum-based decay vessel design; detailed examination of helium-based configurations commenced in 2024 and is addressed in Section 3.

3.1. Design concepts inspired by subterranean tunnel engineering

Under vacuum conditions, the vessel envelope experiences radial external pressure. Cross-sections with circular or other curved geometries were evaluated; buckling performance under external pressure was assessed. Structural concepts inspired by underground tunnel design principles were explored to address this challenge, as depicted in Figure 3.

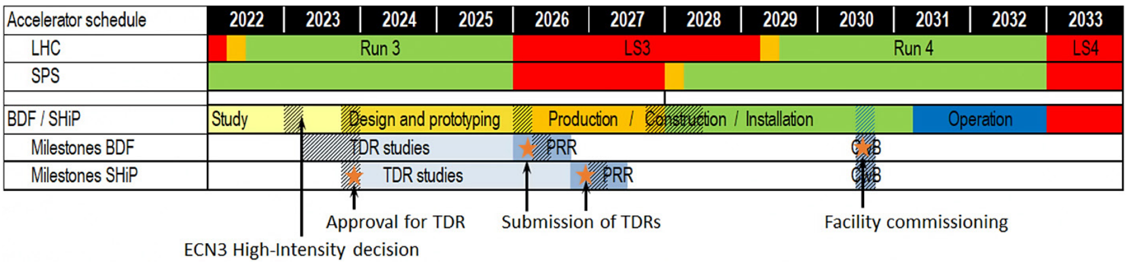

Figure 2. Implementation timeline for Beam Dump Facility of SHiP in ECN3

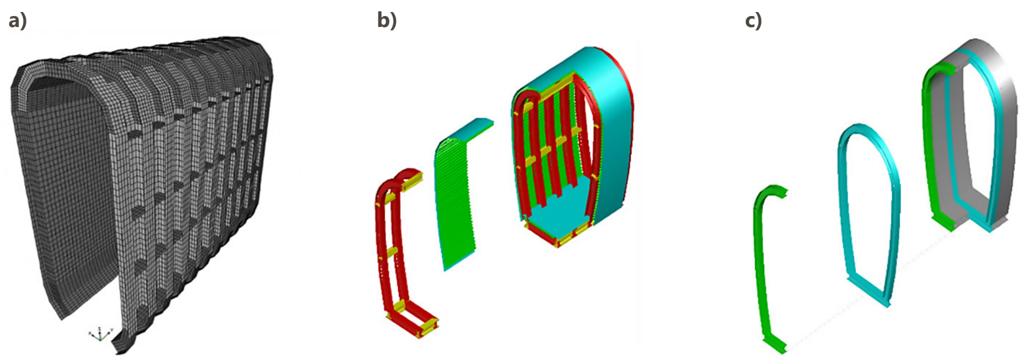

Figure 3. Three finite element models (FEMs) developed with SAP2000 for the earliest design solutions of the decay volume structure

These concepts were represented by three FEMs developed with SAP2000 for the earliest design solutions. SAP2000 was selected for its modeling efficiency for large steel-frame structures and its capability to integrate shell and frame elements directly. Moreover, it offers reliable seismic analysis tools complying with the relevant design standards of the project. These FEMs served as the basis for subsequent structural refinements and informed the design transition toward hybrid RC–steel and fully steel-based vessel configurations. These SAP2000-based FEMs provided the foundation for subsequent validation against experimental prototype tests and guided refinement of vessel wall thickness and stiffening ring placement. Figure 3a depicts a composite steel–concrete design with a layered slab, which was developed to ensure rigidity and resistance to deformation from atmospheric pressure under vacuum conditions. Figure 3b depicts a minimal lightweight alternative of interconnected steel profiles, and Figure 3c depicts a welded steel framework intended to reduce mass; however, these steel-based designs, although lighter than the composite option, exhibited greater flexibility and susceptibility to deformation.

3.2. Structural designs in box-section configuration

To enable SBT integration, the team investigated a system to house liquid scintillator directly against the wall, the outermost steel layer separating the vacuum interior from the environment. Consequently, a modular design of S355JO(J2/K2)W Corten steel segmented into hundreds of cells was developed to contain scintillator. Two successive iterations were proposed, the second refining the first. As of 2025, they represent the most current solutions for the decay vessel in vacuum configuration.

The initial concept, introduced in 2019 and hereafter termed the 2019 Solution, features a box-type structure composed of three key components: inner and outer steel plates; transverse stiffeners; and longitudinal reinforcements. Together these elements constitute a robust, box-like assembly. Following advancements in SBT-related physics performance simulations, revisions to geometry and material thickness were proposed and culminated in the development of the 2024 Solution. Both versions are presented and analyzed in detail in Section 4.2.

4. Decay volume in vacuum and helium configurations

In 2024, significant revisions to the SHiP project requirements prompted new structural concepts, most critically mass optimization and a redefined approach to integrating the liquid scintillator. The reflectivity of the inner wall directly influences light capture within the SBT liquid scintillator modules, which resulted in a proposal to use aluminum. Consequently, the hybrid steel–aluminum design attracted the most attention within the SHiP Collaboration. In this configuration, the steel framework carries structural loads, including lateral forces, whereas aluminum containers serve as non-structural elements that house the liquid scintillator and enhance reflectivity. An additional key development considered helium as an alternative to vacuum within the decay vessel. This configuration eliminates the pressure differential between the interior and exterior of the vessel, i.e., operates at atmospheric pressure (1 atm), and enables the design of a significantly lighter structure. The principles guiding the structural design of the decay vessel are discussed in subsection 4.1, whereas the leading vacuum and helium configuration proposals are presented in subsections 4.2 and 4.3. A flowchart depicted in Figure 4 highlights the adopted design principles and methodology.

The decay vessel design follows a coordinated process beginning with project inputs defined by CERN Coordination requirements (Figure 4), followed by assessment of non-conventional actions typical of particle physics facilities. Interactions with all interfacing subsystems are evaluated to ensure compatibility, thereby enabling the structural design. The final solution undergoes life-cycle optimization to minimize mass and cost while ensuring constructability and sustainability.

4.1. Guidelines and philosophy for design

In accordance with Eurocode 0 (European Committee for Standardization, 2002), three load combinations were applied to assess the decay vessel's structural integrity in terms of stress and deformation: the Ultimate Limit State Combination (UCC), the Serviceability Limit State Combination (SRC), and the Seismic Combination (SSC), as described below.

- The loads acting on the structure in the UCC are calculated as follows:

$$L_{UCC} = 1.35 \cdot (G_1 + G_2 - 1 + G_2 - 2), \quad (1)$$

where G_1 denotes structural loads (dead loads). $G_2 - 1$ represents the radial atmospheric pressure acting on the vessel walls and end caps, approximately 10^{-3} bar. Notably, this pressure does not apply to the helium configuration described in Subsection 4.3, as helium operates at atmospheric pressure and thus produces no pressure differential

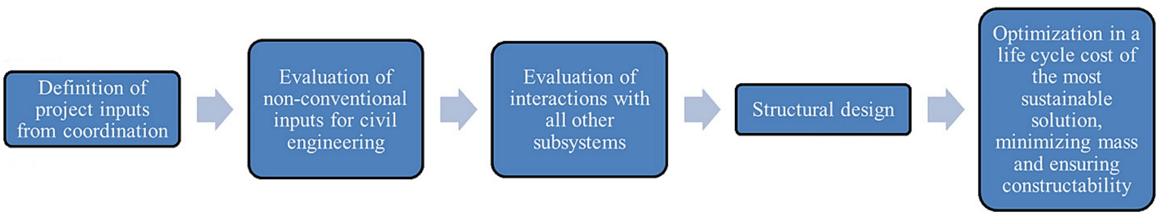

Figure 4. Flowchart of the proposed methodology for the design of the decay vessel

between the interior and exterior of the decay vessel. $G_2 - 2$ corresponds to the load exerted by the liquid scintillator on the longitudinal stiffening elements, assuming a liquid density γ_1 of 900 kg/m^3. To account for potential irregularities, such as transient overpressure or malfunctioning systems, the atmospheric radial pressure component was conservatively amplified by a factor of 1.5.

- Seismic action was considered through the following formulations:

$$L_{SSC1} = G_1 + G_2 - 1 + G_2 - 2 \pm E_x \pm 0.3\ E_y; \quad (2)$$

$$L_{SSC2} = G_1 + G_2 - 1 + G_2 - 2 \pm 0.3\ E_x \pm E_y, \quad (3)$$

where E_y and E_y are the seismic loads in the transversal and longitudinal directions, respectively. Note that Eqns (2) and (3) are alternative formulations for the SSC. The elastic response spectrum Se(T) for the seismic load analysis was defined according to Eurocode 8, Part 1 (European Committee for Standardization, 2004a). The bedrock acceleration was selected ad hoc and set to 0.11 g, whereas the corresponding soil type was classified as Type B. These analysis parameters were defined following internal consultations with CERN's safety departments; notably, the chosen acceleration corresponds to a return period of 475 years. Ongoing investigations aim to further characterize the site's geological conditions and determine the importance factor for the elastic response spectrum.

- The serviceability condition for the SRC is expressed as follows:

$$L_{SRC} = G_1 + G_2 - 1 + G_2 - 2. \quad (4)$$

Temperature effects are neglected because the setup is installed in a controlled underground environment with fluctuations limited to 2–3 °C.

The structural analysis was initially conducted using Robot Structural Analysis Professional (Autodesk, 2019) to corroborate the 2019 Solution for the vacuum configuration described in Subsection 3.2. Subsequently, preliminary manual assessments and a new SAP2000 FEM refined the original model and guided the helium configuration and the updated 2024 Solution for the vacuum configuration.

The steel sheets are modeled as 2D shell elements subjected to two primary in-plane stresses, whereas axial, shear, and bending loads are evaluated through the plate thickness. A fine mesh enhances accuracy. Stress verifications relied on thin-sheet mechanics (Mittelstedt, 2023; Zingoni, 2017). In 2D thin plates, instability depends on: i) structural dimensions, ii) geometry, iii) constraints or boundary conditions, and iv) load type. This approach enhances structural analysis relative to one-dimensional members. To examine instability, we modeled thin rectangular plates simply supported along all four edges and subjected them to compressive loading. This configuration represents the simplest boundary condition for instability modeling and permits direct comparison with an Euler beam. Instability arises when the applied load exceeds a critical threshold. The deformation peaks at the plate's center and tapers toward the edges. Assuming small displacements relative to plate thickness, we employed a potential-energy-based method to calculate the critical load. As outlined in Eurocode 3 (European Committee for Standardization, 2005), the critical stress for a uniformly loaded rectangular plate under in-plane or shear force in vacuum configuration is determined by the following equation:

$$\sigma_c \leq \sigma_{cr,p}, \quad (5)$$

where σ_c denotes the compressive stress. The critical stress $\sigma_{cr,p}$ is defined as follows:

$$\sigma_{cr,p} = k_\sigma \cdot \sigma_E, \quad (6)$$

where k_σ represents the instability constant. It depends on the geometry, applied loads, and boundary conditions. The parameter σ_E is defined as follows:

$$\sigma_E = \frac{\pi^2 E t^2}{12\left(1-\nu^2\right)b^2}, \quad (7)$$

where E represents the Young's modulus, ν denotes the Poisson's ratio, b refers to the dimension of the plate in the direction of the applied load, and t represents the thickness of the plate. The global stress is evaluated using the von Mises criterion based on equivalent stress. Eurocode 3 (European Committee for Standardization, 2005) further addresses the stress path in shell structures. For each plate in the structure, the design equivalent Von Mises stress is derived from the stresses obtained through structural analysis, ensuring equilibrium between the design loads and the internal forces and moments. Specifically, a simplified shell analysis assumes linear elastic material behavior and small deflections, implying that the structure's geometry remains essentially unchanged from its undeformed configuration. Stability verifications evaluate six stress resultants in the shell wall, including axial and shear components. According to Eurocode 3 (European Committee for Standardization, 2005) guidelines, the von Mises equivalent stress σ_{eq} must satisfy the following limit:

$$\sigma_{eq} \leq f_{yd} = \frac{f_y}{\gamma_{st}}, \quad (8)$$

where f_{yd} denotes the steel yielding stress. This design value is selected to prevent excursions into the plastic range. The von Mises equivalent stress σ_{eq} is evaluated as follows:

$$\sigma_{eq} = \sqrt{\sigma_x^2 + \sigma_y^2 + \sigma_z^2 - \left(\sigma_x \cdot \sigma_y + \sigma_x \cdot \sigma_z + \sigma_y \cdot \sigma_z\right) + 3\left(\tau_{xy}^2 + \tau_{yz}^2 + \tau_{zx}^2\right)}, \quad (9)$$

where σ indicates the normal stress and τ denotes the tangential stresses, in the x-, y-, and z-directions.

Additionally, the support structure for the decay vessel and the frames developed for the helium configuration are designed in accordance with Eurocode 3 (European Committee for Standardization, 2005) and Eurocode 8 (European Committee for Standardization, 2004a) guidelines for seismic actions, as outlined below. The design buckling resistance of each compressed steel cross-section was determined by

$$N_{b,Rd} = \frac{X A f_y}{\gamma_{M1}}, \tag{10}$$

where X denotes a reduction factor for buckling, $N_{b,Rd}$ represents the buckling resistance, A denotes the cross-sectional area, f_y refers to the steel yield strength and γ_{M1} denotes a partial safety factor for stability. The bending resistance of the steel members is evaluated as follows:

$$M_{Rd} = \frac{W_{pl} f_y}{\gamma_{M0}}, \tag{11}$$

where M_{Rd} denotes the cross-section design bending resistance, W_{pl} refers to the plastic section modulus, γ_{M0} represents a partial safety factor for uncertainties connected to the material characteristics. Ultimately, the design shear resistance V_{Rd} of the members is assessed as follows:

$$V_{Rd} = \frac{A_v f_y}{\sqrt{3}\gamma_{M0}}, \tag{12}$$

where A_v denotes the shear area of the steel profile.

The deflection of the decay vessel in the vacuum configuration is verified to ensure the maximum plate displacement remains below H/250, where H denotes the plate height. As this limit is typically applied to civil structures solely for serviceability, it may be revised during the final executive design phase of the project. In that phase, technical details such as the number of bolted connections between elements, welding operations, and the quantity of cables required to fill the decay vessel with liquid scintillator will be addressed. The EN-13445 standard (European Committee for Standardization, 2004b) will be applied with particular attention to vacuum containment requirements. Nonetheless, the design solutions presented in Subsections 4.2 and 4.3 for the vacuum and helium configurations, respectively, are considered structurally complete. The primary uncertainties originate from ongoing physics investigations aimed at optimizing the geometrical envelope.

4.2. Decay vessel configuration for vacuum

Over the past decade, several vacuum decay vessel designs were explored before reaching final consensus on a structure fabricated from S355JO(J2/K2)W Corten steel. Section 4 briefly summarizes the solutions described in detail by Miano et al. (2020). Subsection 4.2.1 outlines the design proposed by Miano et al. (2020), referred to as the 2019 Solution, and Subsection 3.2.2 presents its subsequent updates.

4.2.1. Design solution as of 2019

The structural design of the decay volume, finalized in 2019, employed a box section of S355JO(J2/K2)W Corten steel elements. This section comprised three main components: (1) inner and outer steel sheets, each 20 mm thick except along the final 16.4 m, where thickness increased to 30 mm; (2) transverse stiffeners spaced at 800 mm intervals, 10 mm thick and approximately 400 mm high, with height reduced to 300 mm over the initial 14.4 m to comply with the deflected muon background envelope, increased to 410 mm over the subsequent 19.2 m, and set at 390 mm along the last 16.4 m; (3) longitudinal stiffeners, 10 mm thick, with spacing varying between 804 and 1702 mm. The detailed drawings and specifications are provided in Miano et al. (2020).

4.2.2. Design solution as of 2024

The decay volume design for the 2024 Solution builds upon the 2019 Solution, introducing improvements in multiple areas. Steel structures suit earthquake-prone regions owing to their low weight, flexibility, and energy-absorption capacity. They enable rapid on-site assembly, precise construction, and straightforward modification and repair. This assembly approach employs reversible connections between structural components, which enhance environmental sustainability through potential recyclability, facilitating disassembly and component reuse. To refine the initial design, several iterations were conducted to identify the most suitable structural improvement. The key factors considered during this process include: i) the requirement to house the liquid scintillator in specific engineered compartments throughout the decay volume; and ii) the need to minimize steel plate thickness.

As in the box section described in Section 3.2.1, the 2024 Solution also utilizes S355JO(J2/K2)W Corten steel elements but incorporates the following complete detailed geometry updates:

- Transverse stiffening members are spaced 820 mm apart, except for the last cell at Z = 0, where spacing is reduced to 800 mm because of the smaller cross-section.
- These members have a thickness of 15 mm and a height of approximately 240 mm.
- The longitudinal stiffening elements have a thickness of 15 mm, with spacing ranging from 800–1700 mm, respectively.

The final cross-section of the decay volume at Z = 50 m is illustrated in Figure 5a). The internal steel sheet measures approximately 6 m × 4.0 m, whereas the external steel sheet measures about 6.48 m × 4.48 m. The initial cross-section at Z = 0 m is depicted in Figure 5b), where the internal steel sheet dimensions are 1 m × 2.7 m, and the external sheet measures approximately 1.48 m × 3.18 m. These dimensions have been significantly reduced compared to those in Miano et al. (2020). This design optimization maximizes the available space for the liquid scintillator detector, permitting the use of 854 compartments instead of the 1848 used in the 2019 Solution.

Furthermore, a test-beam prototype (Ehlert et al., 2019) accurately demonstrated that the overall dimensions of the decay vessel structure, approximately 820 mm × 1200 mm, are feasible. The decay volume structure itself weighs around 350 tons. The load-bearing structure primarily consists of an internal steel plate reinforced by welded transverse stiffeners arranged in two perpendicular directions. This type of structural design is common in bridge

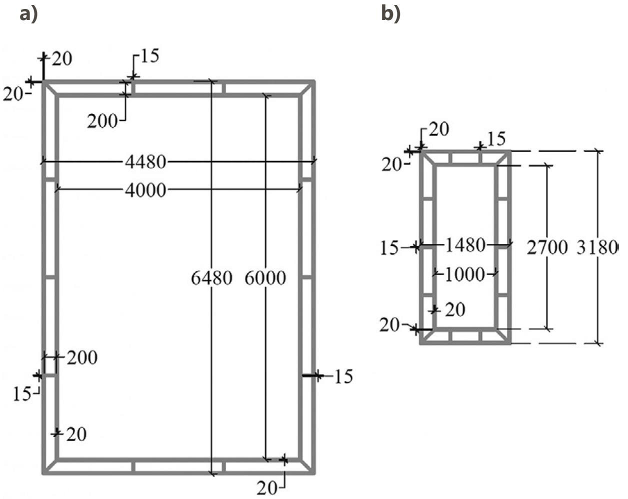

Figure 5. Decay vessel cross-sections: a – large cross-section near the SND (at Z = 50 m); b – small cross-section near the decay spectrometer (at Z = 0 m)

and ship construction; thus, the proposed design for the decay vessel can be categorized as a welded cross-section steel structure. Notably, longitudinal stiffeners minimize compartment height, and an outer steel plate encloses the liquid scintillator, forming a box-shaped section. Stiffening elements interconnect the two steel plates to enhance the strength of the sections in the transverse direction, effectively mimicking the behavior of a box with inner and outer steel sheets working at comparable stress levels. The transverse stiffeners are uniformly spaced at 820 mm intervals. In the longitudinal direction, however, interaction between the inner and outer sheets is reduced, as the longitudinal stiffener spacing varies from approximately 1000 mm at the small cross-section (Z = 0 m) to 1500 mm at the large cross-section (Z = 50 m). Consequently, the double-wall structure cross-section changes along the 50 m length of the decay vessel.

Thus, the global behavior of the decay vessel in the transverse direction follows the structural performance of a box, as the internal and external steel plates experience similar stress paths of the same order of magnitude. This condition is primarily governed by the dimensions of the transverse stiffening members, which are spaced only 800 mm apart. However, this condition is not observed in the longitudinal direction, where the distance between longitudinal stiffening members ranges from 800 mm to 1700 mm. For conciseness, stress paths are omitted because they match those previously presented (Miano et al., 2020) in their shape and magnitude.

An aluminum bolted wall seals the upstream end of the decay volume, whereas a bolted flange attaches the downstream end to the spectrometer section's vacuum chamber. Supports positioned approximately 5 meters apart beneath the vessel consist of HE steel profiles combined with tubular profiles, as depicted in Figure 6. The HE steel profiles are arranged to distribute loads uniformly.

This support system prevents vertical and transverse displacements while permitting limited longitudinal movement under compressive forces. The downstream section connects via the spectrometer section to the spectrometer magnet, which serves as the fixed point for the entire assembly.

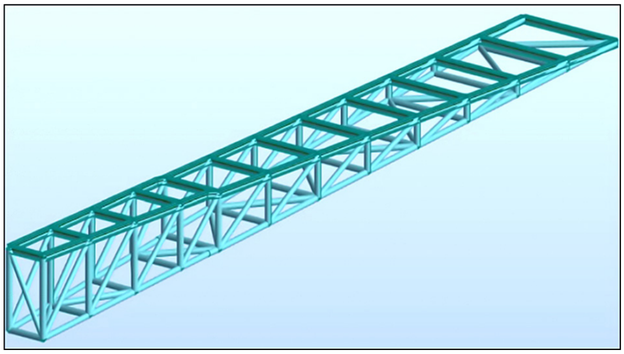

Figure 6. Sketch of the support system, which consists of HE steel profiles and circular steel profiles

4.3. Helium configuration

As discussed earlier, the SHiP collaboration selected helium at 1 atm to fill the decay vessel after extensive discussion, aiming to minimize the mass interacting with decaying particles. This choice balances mass reduction and the requirement for a lightweight vessel capable of withstanding atmospheric pressure. Although a vacuum configuration provides the best performance for the experiment, particularly for dark matter detection, helium at 1 atm offers a much lighter structural design for the decay vessel. Accordingly, the structural design strategy decouples the decay vessel into two separate systems: i) a steel structural system and ii) aluminum boxes. The steel structure bears all loads, including those from the liquid scintillator and seismic forces, whereas the aluminum boxes contain the liquid scintillator. Using aluminum instead of steel reduces the decay vessel's weight and enhances particle detection. Initially, applying aluminum coating on steel was considered; however, this approach proved suboptimal owing to accelerated material degradation. The design guidelines for the decay vessel in the helium configuration follow those established for the vacuum configuration. Notably, the term $G_2 - 1$ in Eqns (1)–(4) becomes zero under helium, which yields significant material savings. Consequently, the external steel sheet employed in the vacuum configuration (Subsection 4.2) has been eliminated, and the number of scintillator boxes has been drastically reduced to 136. A schematic of the steel framework proposed for the decay vessel in the helium configuration is illustrated in Figure 7.

The internal cross-sectional dimensions remain unchanged relative to the vacuum configuration of the 2024 Solution presented in Figure 5: the larger rectangular cross-section measures 4000 mm × 6000 mm, whereas the smaller section measures 1000 mm × 2700 mm. Figure 7 depicts HE200B stiffening members that support the aluminum containers and create space for bolts. The structural profiles were de-signed and verified using SAP2000;

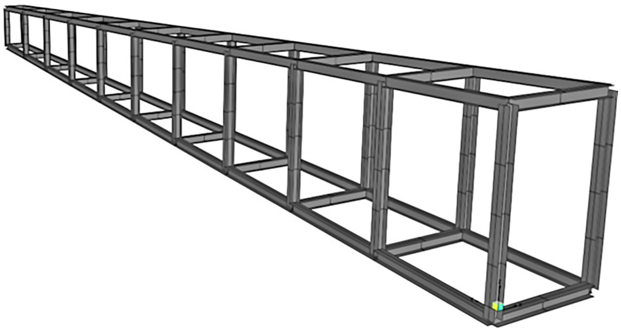

Figure 7. Sketch of the proposed steel frame of the decay vessel in the helium configuration

Figure 8 presents the deformed shapes of the decay vessel under a) dead loads, b) Ex seismic action, and c) Ey seismic action.

The stress levels in all vessel sections were verified; however, the safety checks outlined in Eqns (5)–(9) are omitted here for brevity. These verifications are available upon reasonable request to the authors. Below, the key outcomes of the safety assessment for both the Ultimate Condition Combination (UCC) and the Seismic Combination (SSC), as introduced in Subsection 4.1, are presented. The maximum ratio between the applied stress and the critical (allowable) stress, referred to as the demand-over-capacity ratio (D/C), was computed across the entire surface of each plate and determined for buckling stress conditions. The verification process accounted for each member's longitudinal orientation and centroid position within the global reference frame, as stress distribution depends on both factors.

Because of symmetry along the x- and y-axes, stress distribution across all plates at a given longitudinal position remains consistent. The stress verification results for both the Ultimate Condition Combination (UCC) and the Seismic Combination (SSC) demonstrate that the entire structure remains within globally safe limits. The demand-over-capacity (D/C) ratio for the plates typically varies between 0.3 and 0.7 for both buckling and Von Mises equivalent stress assessments, according to Eqns (5) and (8).

Localized stress concentrations occur near boundaries and corners, where the D/C ratio can reach 0.95, likely owing to modeling artifacts rather than actual structural deficiencies. These artifacts will be addressed in subsequent design phases, particularly during the executive phase. In this context, the SHiP collaboration will conduct detailed investigations employing refined modeling techniques to accurately capture the structural behavior in these critical regions.

Figure 9 depicts the first four mode shapes of the steel structural component of the decay vessel, obtained from SAP2000 analysis, corresponding to fundamental vibration periods: a) T_1 = 0.46 s; b) T_2 = 0.40 s; c) T_3 = 0.37 s; and d) T_4 = 0.31 s. which respectively correspond to f_1 = 2.17 Hz, f_2 = 2.50 Hz, f_3 = 2.70 Hz, and f_4 = 3.23 Hz. The liquid scintillator is considered in the analysis. The behavior of the decay vessel is prominently visible in Figure 9c), where the considerable seismic mass of the liquid induces noticeable bending in the lateral walls of the decay vessel. In contrast, the first two mode shapes correspond to the lateral deflections of the structure, where the square frames formed by the transverse stiffening members behave similarly to moment-resisting frames, thereby offering substantial lateral stability. The fourth mode shape highlights the pulsating effect of the seismic mass of the liquid scintillator.

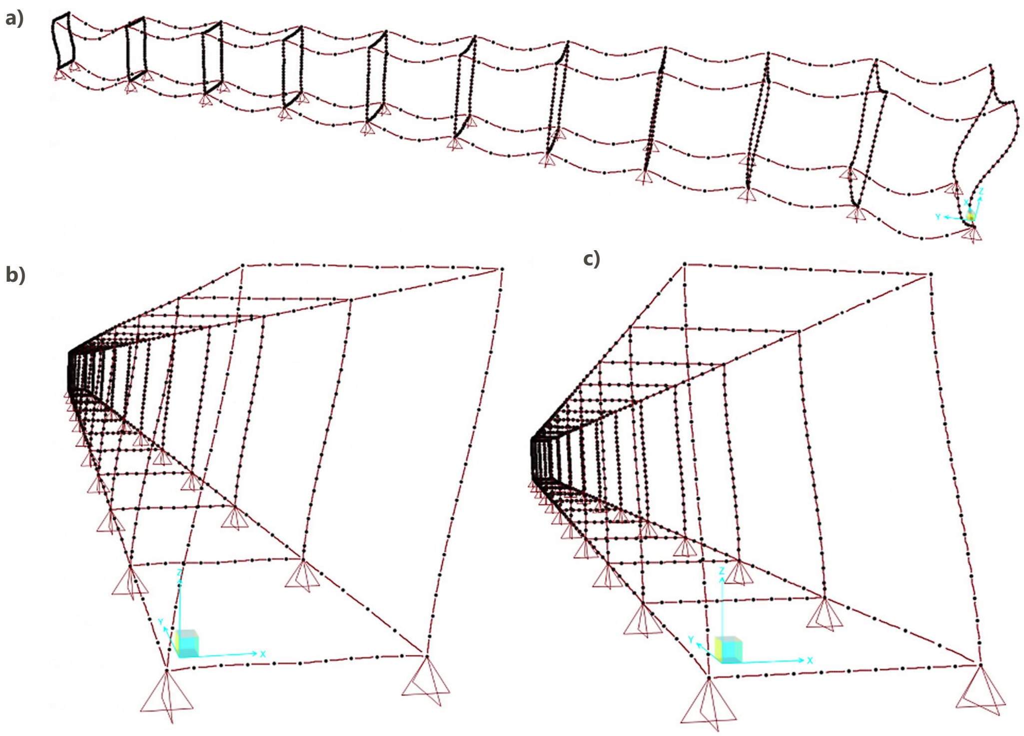

Figure 8. Deformed shapes of the decay vessel for: a – dead loads; b – Ex seismic action; c – Ey seismic action

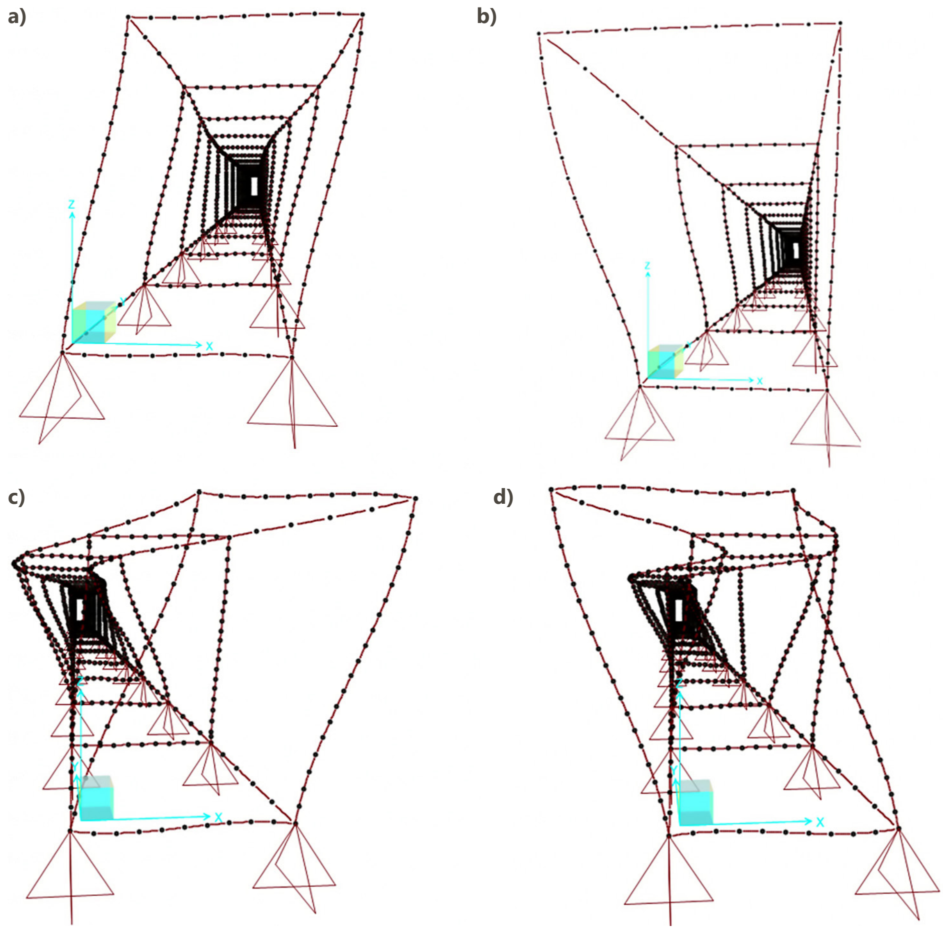

Figure 9. First four mode shapes of the steel structural component of the decay vessel, obtained from SAP2000 analysis, corresponding to the fundamental periods of vibration: a – T_1 = 0.46 s; b – T_2 = 0.40 s; c – T_3 = 0.37 s; d – T_4 = 0.31 s

Although omitted here for conciseness, all verification checks required by Eurocode 3 (European Committee for Standardization, 2005) and Eurocode 8 (European Committee for Standardization, 2004a), summarized in Eqns (5)–(12), have been satisfied for both helium and vacuum configurations. The vacuum configuration's most critical load case corresponded to the Ultimate Limit State Combination (UCC) defined in Eqn (1), which expresses the dominant factor of radial atmospheric pressure G_2 – 1 acting on the vessel walls and end caps, rendering seismic effects negligible. Conversely, in the helium configuration, the Seismic Combination (SSC) governed the design, and Eqns (2) and (3) guided the steel frame layout. The helium configuration employs a support structure composed of column pairs positioned at the transverse stiffening-member locations, ensuring direct support to the decay vessel, as illustrated in Figure 7. This arrangement differs from the vacuum-configuration support system depicted in Figure 6. A preliminary structural design was developed for this configuration employing HE220A steel profiles. The cross-section and relevant geometric dimensions of the HE220A profile are displayed in Figure 10.

The support structure design adhered to Eurocodes 3 and 8 guidelines, as detailed in Subsection 4.1. The principal verification steps encompassed buckling, bending, and shear-resistance assessments. The steel frame was arranged into compartments to accommodate aluminum containers holding the liquid scintillator for particle detection (Rössing et al., 2024). A typological external view of an aluminum container is presented in Figure 11.

The decay vessel design is exhibited in Figure 7, wherein the primary structural steel frame is decoupled from the aluminum containers that serve a non-structural role. The aluminum boxes, engineered to house the liquid scintillator, are not intended to bear dead loads. Bolted connections along the container edges secure the aluminum boxes to the decay vessel's transverse stiffening members, as illustrated in Figure 11. This modular arrangement offers flexibility for potential updates to seismic action parameters, which remain under investigation. The decoupled configuration comprises a load-bearing steel frame and independent aluminum containers. This separation permits adjustments to the steel components without altering the container design, thus preventing disruptions to ongoing physics simulations. In recent years, aluminum alloys have been increasingly used in the construction industry due to their favorable properties. For the SHiP experiment, aluminum has been selected based on its excellent performance in particle detection. Several alloy options have been evaluated for this application (Georgantzia et al., 2021), although the final selection is pending.

h [mm]	b [mm]	t_w [mm]	t_f [mm]	r [mm]	d [mm]	h_1 [mm]	i_z [mm]	i_y [mm]	Ø [mm]	S_s [mm]	p [mm]
210	220	7	11	18	152	188	5.51	9.17	M27	50.09	103

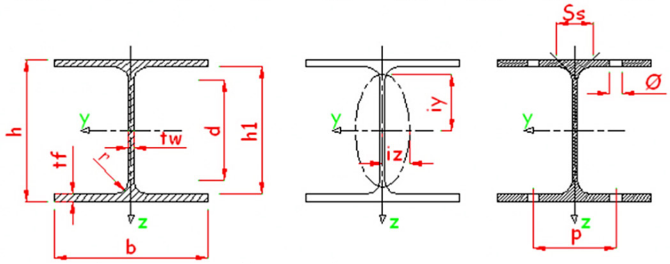

Figure 10. Cross-section and relevant geometrical dimensions of the HE220A steel profile used in the support system. All dimensions are provided in millimeters (mm)

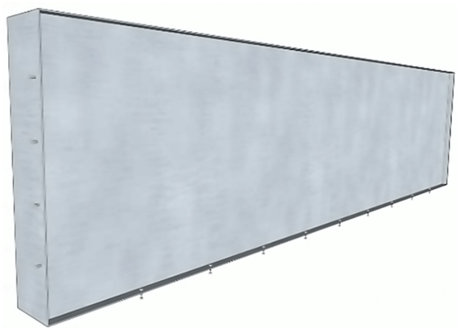

Figure 11. Typological external view of an aluminum container

The optimization of a hybrid structural system composed of a steel load-bearing frame and aluminum box modules requires an integrated, multidisciplinary approach that leverages advanced numerical modeling, material–structure interaction analysis, and manufacturing feasibility criteria. Notably, the primary objective is to minimize the total system mass while ensuring adequate stiffness, mechanical resistance, and global stability without compromising constructability or exceeding cost constraints. From a structural engineering perspective, the steel frame constitutes the primary load-bearing subsystem, providing high strength and stiffness. The design mandate required elastic behavior; consequently, ductility was not evaluated. Integrating aluminum box units introduces critical connection design requirements. Accurate assessment is essential to predict load transfer mechanisms and local stress concentrations at these joints.

Ultimately, optimizing the steel-frame–aluminum-box hybrid structure requires a systems-engineering workflow that integrates structural mechanics, manufacturing science, and economic analysis. This approach yielded a mass-efficient, high-performance, and cost-effective design compatible with industrial fabrication and assembly constraints.

5. Design of pumping system, filling, and emptying procedures

The pumping system fills and subsequently empties the scintillator boxes surrounding the vessel with liquid scintillator, considering the configuration described in Section 3.3, adopted for helium operation. The liquid scintillator (LS) adopted to detect muons entering the decay vessel is a mixture of linear alkylbenzene (LAB) and 2 g/L 2.5-diphenyloxazole (PPO). It has a density of 856 kg/m^3 and a dynamic viscosity of 6.24×10^{-3} Pa·s (Alt et al., 2024). As described, the steel structure bears the loads and houses the aluminum boxes designed to contain the scintillator. These boxes (Figure 12) are 5 m long and 0.020 m wide. They are bolted to the frame to cover its entire surface, forming ten rings (Figure 12). Each ring comprises two C-shaped semi-rings (left and right), each consisting of a bottom horizontal box, four vertical boxes, and a top horizontal box, totaling $6 \times 2 = 12$ boxes per ring (Figure 13). To accommodate the particle detectors, each box is internally subdivided into five 1 m compartments, with one compartment allocated for each sensor.

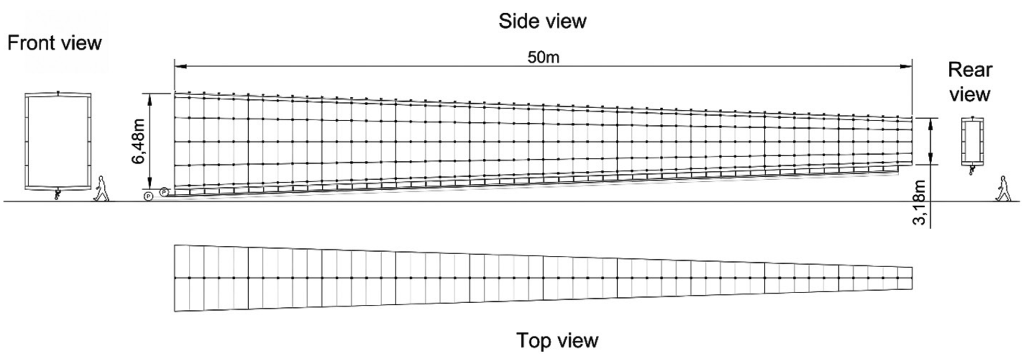

Figure 12. General scheme of the structure, with filling and discharge circuits (front, side, rear and top views)

As stated, the main constraint of the filling design is to avoid air pockets larger than a few micro-bubbles; the maximum allowable bubble diameter is 10 mm. Therefore, the pumping system delivers liquid from the bottom to the top of the rings to facilitate air exit. Moreover, the filling procedure must employ an appropriate velocity to prevent vortex formation and air entrapment, especially at the edges.

The hydraulic circuit links the reservoir, which holds 137 m^3 of liquid, to the vessel via a main steel pipe placed beneath the structure and is driven by a single pump. The system fills the rings sequentially, one at a time, and uses valves to isolate sections. In each ring, the two C-shaped semirings fill simultaneously as liquid rises in the five separate compartments. Liquid is introduced into each semiring through five inlet pipes, each connected to a bottom compartment, while five vents at the top enable air release and permit thermal expansion during temperature increases (Figure 13). The general scheme of the structure encompasses the front, side, rear, and top views of the vessel, illustrating the filling and discharge circuits.

To facilitate the exit of air that naturally migrates upward, the bottom compartments are realized with a transversal slope of 3.3% from the vessel's center toward the outer side, as depicted in Figure 13. The input pipes connected to the bottom boxes are located at the lowest part of each compartment, as illustrated in Figures 13–15. Analogously, the top compartments are realized with the same transversal slope, resembling a pitched roof, with vents placed at their highest part, as depicted in Figure 13.

The compartments of each ring are vertically connected through holes, the number of which constitutes a design parameter. Moreover, when establishing connections between the boxes, the risk of liquid leakage must be carefully considered. Therefore, the connections are implemented via external pipes, as presented in Figure 13 and Figure 15. Each connection includes a valve that can be closed in case of failure to isolate a box and reduce or prevent liquid leakage. The rear section of the structure with all 12 boxes and the emptying and filling circuit is depicted in Figure 13, whereas the details of the hydraulic circuits and the external connections between the boxes are presented in Figure 15.

A total input discharge from the hydraulic circuit entered each semiring and was divided equally among the five input pipes. The fluid then rose horizontally in the bottom compartments, and once they were filled, moved to the lowest vertical compartments through the holes and connecting pipes, and similarly for the upper boxes.

The input discharge, hole size, and number of holes and connecting pipes were determined by imposing three constraints. First, the filling velocity, defined as the rate at which the liquid level rises in the box, had to remain below the maximum allowable air bubble rise speed. Second, the Reynolds number for flow through each hole and each connecting pipe was maintained below the turbulent-regime threshold ($<10^{-4}$) to prevent vortex formation that could entrap air. Third, head losses were limited in magnitude. The system design and filling procedure were developed by first considering the tallest ring, with the section depicted in Figure 5a. Overall, to achieve a filling time of approximately 1 h per ring, the total input discharge was fixed at 5.4 l/s per ring. Accordingly, this flow was equally divided among ten input pipes (five per semiring), each with D = 1'' (internal diameter 27.3 mm). Notably, the liquid velocity and Reynolds number in each input pipe were 0.92 m/s and 3.4×10^3, respectively. The compartments exhibiting the highest filling velocity are located on the lateral side of the ring and have a horizontal section of

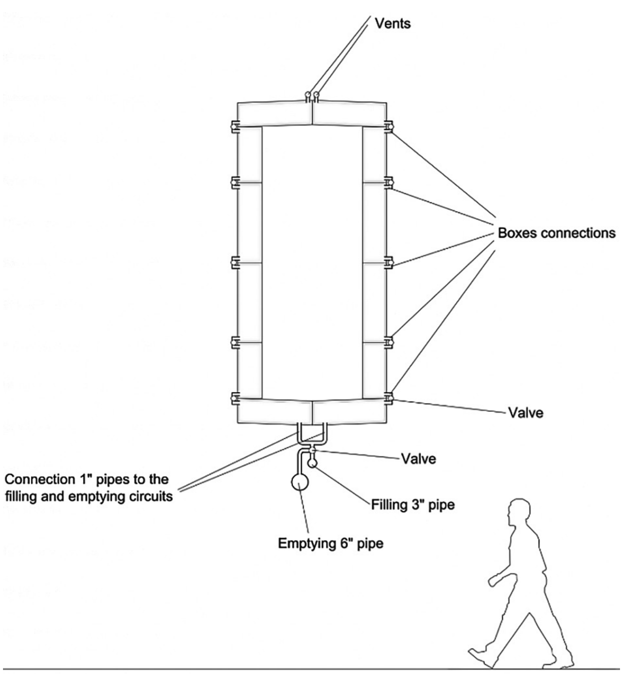

Figure 13. Rear section of the structure, with all the 12 boxes

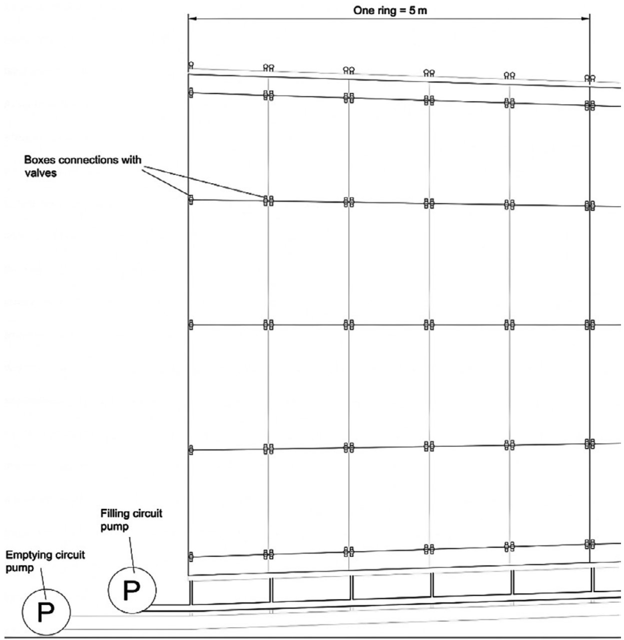

Figure 14. Close-off view of the first ring, with the filling and emptying circuits placed below the structure

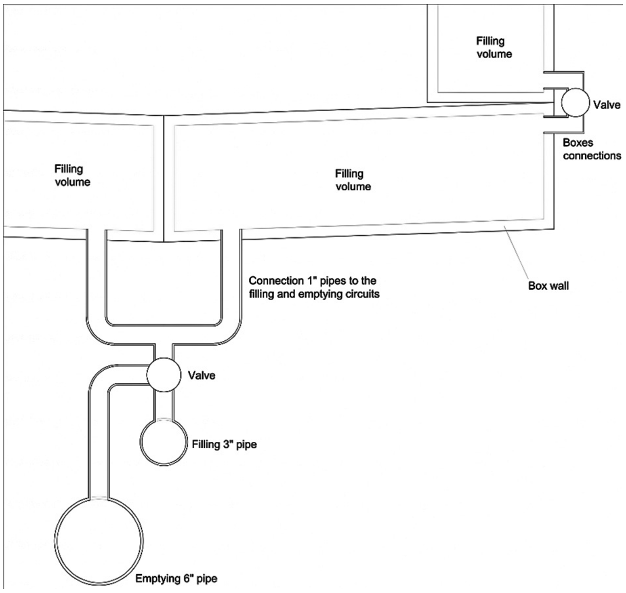

Figure 15. Particular of the filling and emptying hydraulic circuit below the rear section. The wall of the boxes and the connection between the bottom and the first vertical box is also visible

1000 × 200 mm. In these compartments, each input pipe supplied an inlet discharge of 0.54 l/s, and the filling velocity reached 2.69 mm/s, which is lower than the rising velocity of an air bubble with diameter 10 mm. Specifically, using the same total input discharge, the smaller ring presented in Figure 5b filled in 25 min; thus, the entire structure required approximately 7 h in total. Notably, considering two connecting pipes per compartment with D = 1'', the liquid flow velocity and Reynolds number in each were 0.46 m/s and 1.7×10^3, respectively. The local head loss per pipe under these conditions was 0.011 m.

The supply line connecting the pumping system to the rings had D = 3'' (83.1 mm), corresponding to a flow velocity of 1 m/s under nominal operating conditions. The pump is located in the circuit adjacent to the tallest ring, and power is evaluated as (Gülich, 2010):

$$P = \frac{\gamma Q H_m}{\eta}, \tag{13}$$

where γ denotes the specific weight of the liquid, η = 0.6 symbolizes the pump efficiency, Q indicates the inlet discharge, and H_m denotes manometric head. H_m comprises the geodetic elevation difference (7 m for the tallest ring) and head losses. The local head loss is computed by summing losses in all pipes and connections, which equals 1 m. The continuous head loss is calculated via the Darcy–Weisbach formula (White, 2016):

$$H_c = \frac{\lambda V^2}{2gD} L, \tag{14}$$

where D and L denote the diameter and length of the pipe, respectively, V indicates the pipe velocity, g indicates the gravity. λ denotes the friction factor expressed through the following formula:

$$\frac{1}{\sqrt{\lambda}} = -2 \log\left(\frac{2.51}{Re\sqrt{\lambda}} + \frac{\epsilon / D}{3.71}\right) L. \tag{15}$$

Assuming pipe roughness ε = 0.03, the continuous head loss is 0.92 m. Substitution into Eqn (13) yields 0.8 kW pump power. A volumetric pump was selected to accommodate variability in head loss from differing ring distances and heights.

However, during filling, lower compartments bear the overlying liquid, resulting in elevated pressure that increases load on container walls and necessitates thicker aluminum. This condition poses challenges in the taller rings of the structure. As an alternative configuration, the semiring can be divided into two L-shaped modules that are filled separately. This solution is still under development. In this configuration, additional input pipes connected to the circuit would be required.

In an emergency, the liquid must be removed quickly from the rings through the section of the circuit devoted to emptying. Each compartment has one output pipe, identical in size to the input, installed at the bottom and equipped with a valve. The liquid discharged through these output pipes collects in a closed circular channel beneath the structure. The output circuit is equipped with a pump that transfers the liquid to a reservoir outside the laboratory. The emptying time is a design parameter: with a 6-inch pipe and a flow velocity below 2 m/s, emptying the entire volume requires under 1 hour. During emptying, vents at the top open to allow air inflow as the liquid exits from the bottom. Valve and vent operations are activated by a remote control system.

6. Conclusions

The structural design approaches for the decay vessel differ substantially between vacuum and helium configurations because of the objective to minimize mass interacting with particles. In the vacuum setup, the vessel must withstand a 1 atm pressure differential between interior and exterior. The helium configuration operates at atmospheric pressure without a pressure differential, which permits a significantly lighter structure. It employs a single steel plate matching the size of the internal plate used in the 2024 vacuum configuration, as depicted in Figure 7. The setup further includes fewer compartments and a significantly reduced number of both transverse and longitudinal stiffening components. The external plate in the helium configuration consists of a thin, non-structural, lightweight aluminum sheet. The boxes housing the liquid scintillator are fabricated from aluminum, which enhances detection efficiency and significantly reduces material usage. Consequently, the total mass decreases from 350 tons in the 2024 vacuum solution to approximately 160 tons in the structural design of the helium configuration.

In this regard, the optimization strategy applied to both the structural and hydraulic design processes has significantly strengthened the effectiveness of the experiment and its core objectives. A multidisciplinary team including structural engineers, hydraulic engineers, and experimental physicists, among others, collaborated closely to develop an optimal decay vessel structure that minimizes the interaction between its mass and the dark matter targeted for detection. In the context of large-scale international collaborations such as SHiP, a specifically multidisciplinary, robust, and comprehensive integrated approach as proposed in this article for the decay vessel is essential. Accordingly, the proposed design approach separates the mechanical system into two primary components: a structural steel framework for the decay vessel and non-structural elements, such as the aluminum boxes. This separation permits flexibility if seismic conditions evolve during the project, as ongoing detailed analyses of soil stratigraphy across the site and seismic wave transmission through subsurface ground layers are expected to prompt reevaluation of the seismic loads applied at this stage.

The aluminum boxes will be installed using a mobile hydraulic cylinder system in the initial design, such that sufficient space for transportation and operations beneath the vessel is ensured in both longitudinal and transversal directions. This approach contrasts markedly with the 2024 Solution, in which the entire steel structure of the decay vessel served the dual purpose of providing structural support for all vertical and lateral loads and housing the liquid scintillator compartments. Consequently, no external non-structural components were added later, and the support system comprised an assembly of HE and tubular steel profiles forming a truss-like framework, as depicted in Figure 5. In this context, decoupling the aluminum boxes offers clear benefits, as they remain unaffected by potential changes in seismic loads. Moreover, it enables independent physics performance simulations without affecting the structural steel framework designed to withstand dead loads and seismic forces. Another notable change in the helium configuration concerns the support system: the supports are designed to provide uninterrupted, convenient access to the bottom of the decay vessel, as depicted in Figure 7.

The aluminum boxes will be installed using a mobile hydraulic cylinder system, which ensures ample space for transportation and operation beneath the vessel in both longitudinal and transverse directions. This approach contrasts with the 2024 Solution, where the entire steel structure of the decay vessel served a dual role: providing structural support for all vertical and lateral loads and containing the liquid scintillator compartments. Consequently, no additional external non-structural elements were required, and the support system was designed as a truss-like assembly composed of HE and tubular steel profiles, as depicted in Figure 5.

Notably, the complexity, multidisciplinary scope, and scale of the SHiP project created substantial challenges for conventional structural design approaches. Mass minimization was addressed through topology optimization and parametric sizing studies. Constructability considerations steered the optimization toward practical solutions, accounting for fabrication tolerances, weld accessibility, bolted connection standardization, and assembly sequencing requirements. Differences in weldability and connections between steel and aluminum were resolved through appropriate detailing. Modularization of the aluminum boxes can further enhance manufacturing efficiency and reduce on-site labor time. Cost containment was ensured by integrating material cost models, fabrication and assembly metrics, and maintenance projections into the optimization loop. Sensitivity analyses will identify the cost drivers associated with the selected solutions.

The study of the hydraulic circuit and filling procedure recommends introducing liquid from bottom to top, which facilitates the escape of air that naturally rises. Vertical emptying similarly ensures rapid discharge of liquid by gravity. The findings demonstrate the necessity of selecting precise valves and vents and reveal two drawbacks of the current solution: high pressure in the lower compartments and potential leaks. Consequently, further research must address an ad hoc design for valve connections between the boxes.

Although the authors consider the proposed approach optimal at this stage, they are evaluating alternative options while accounting for cost and logistical constraints. Another limitation arises from the project's ongoing status and the evolving design requirements, which prevent full automation of the structural design workflow. Therefore, the process must proceed incrementally and iteratively, with stepwise verification of load cases, boundary conditions, detailing, and constructability constraints, as required in complex civil engineering structures characterized by tight tolerances and strong subsystem interdependencies.

Funding

This research received no external funding.

Data availability statement

Data will be made available upon reasonable request.

Conflict of interests

The authors declare that there is no conflict of interest.

Ethical approval

This article does not contain any studies with human participants or animals performed by any of the authors.

Authors' contribution

All authors contributed to the study conception and design. Material preparation and data collection were performed by Fabrizio Aloschi. Structural analyses were performed by Fabrizio Aloschi, Andrea Miano, and Antimo Fiorillo. Hydraulic analyses were performed by Oreste

Fecarotta, Cristiana Di Cristo, and Giuseppe Del Giudice. Giovanni De Lellis, Richard Jacobsson, and Andrea Prota supervised the work. The original draft of the manuscript was prepared by Fabrizio Aloschi and all authors commented on previous versions of the manuscript. All authors read and approved the final manuscript.

References

Abbaneo, D., Acampora, G., Ahmad, S., Albanese, R., Alexandrov, A., Alicante, F., Aloschi, F., Androsov, K., Anokhina, A., Asawatangtrakuldee, C., Ayala Torres, M. A., Bangaru, N., Battilana, C., Bay, A., Bertocco, A., Betancourt, C., Bick, D., Biswas, R., Blanco Castro, A., ... Zamora Saa, J. (2025). Installation and performance of the 3rd veto plane at the SND@LHC detector. *Journal of Instrumentation*, *20*(7), Article P07011. https://doi.org/10.1088/1748-0221/20/07/P07011

Ahdida, C., Akmete, A., Albanese, R., Alt, J., Alexandrov, A., Anokhina, A., Aoki, S., Arduini, G., Atkin, E., Azorskiy, N., Back, J. J., Bagulya, A., Baaltasar Dos Santos, F., Baranov, A., Bardou, F., Barker, G. J., Battistin, M., Bauche, J., Bay, A., ... Zimmerman, J. (2022). The SHiP experiment at the proposed CERN SPS beam dump facility. *The European Physical Journal C*, *82*(5), Article 486. https://doi.org/10.1140/epjc/s10052-022-10346-5

Alshibani, A., Almuhtaseb, O., Mohammed, A., & Ghaithan, A. M. (2024). A regression-based model for parametric cost estimation of industrial steel structures. *Journal of Civil Engineering and Management*, *31*(1), 71–84. https://doi.org/10.3846/jcem.2024.22472

Alt, J., Bezshyyko, O., Böhles, M., Brignoli, A., Conaboy, A., Deucher, P., Eckardt, C., Ernst, A., Fischer, H., & Hollnagel, A. (2024). Performance of a first full-size WOM-based liquid scintillator detector cell as prototype for the SHiP Surrounding Background Tagger. *Journal of Instrumentation*, *19*, Article P05024. https://doi.org/10.1088/1748-0221/19/05/P05024

Autodesk. (2019). *Software*.

European Committee for Standardization. (2002). *Eurocode 0*: *Basis of structural design* (EN 1990). Brussels.

European Committee for Standardization. (2004a). *Eurocode 8*: *Design of structures for earthquake resistance – Part 1*: *General rules*, *seismic actions and rules for buildings* (EN 1998-1:2004). Brussels.

European Committee for Standardization. (2004b). Unfired pressure vessels (EN 13445). Brussels.

European Committee for Standardization. (2005). *Eurocode 3*: *Design of steel structures – Part 1-3*: *General rules–Supplementary rules for cold-formed members and sheeting* (EN-1993-1-3). Brussels.

Coronado-Hernández, O. E., Fuertes-Miquel, V. S., Besharat, M., & Ramos, H. M. (2018). Subatmospheric pressure in a water draining pipeline with an air pocket. *Urban Water Journal*, *15*(4), 346–352. https://doi.org/10.1080/1573062X.2018.1475578

De Martino, G., Fontana, N., & Giugni, M. (2008). Transient flow caused by air expulsion through an orifice. *Journal of Hydraulic Engineering*, *134*(9), 1395–1399. https://doi.org/10.1061/(ASCE)0733-9429(2008)134:9(1395)

Ehlert, M., Hollnagel, A., Korol, I., Korzenev, A., Lacker, H., Mermod, P., Schliwinski, J., Shihora, L., Venkova, P., & Wurm, M. (2019). Proof-of-principle measurements with a liquid-scintillator detector using wavelength-shifting optical modules. *Journal of Instrumentation*, *14*(3), Article P03021. https://doi.org/10.1088/1748-0221/14/03/P03021

Elmousalami, H. H. (2020). Artificial intelligence and parametric construction cost estimate modeling: State-of-the-art review. *Journal of Construction Engineering and Management*, *146*(1), Article 03119008. https://doi.org/10.1061/(ASCE)CO.1943-7862.0001678

Fuertes-Miquel, V. S., Coronado-Hernández, O. E., Iglesias-Rey, P. L., & Mora-Meliá, D. (2019). Transient phenomena during the emptying process of a single pipe with water–air interaction. *Journal of Hydraulic Research*, *57*(3), 318–326. https://doi.org/10.1080/00221686.2018.1492465

Georgantzia, E., Gkantou, M., & Kamaris, G. S. (2021). Aluminium alloys as structural material: A review of research. *Engineering Structures*, *227*, Article 111372. https://doi.org/10.1016/j.engstruct.2020.111372

Gülich, J. F. (2010). Operation of centrifugal pumps. In *Centrifugal pumps* (pp. 665–714). Springer. https://doi.org/10.1007/978-3-642-12824-0_11

Hou, Q., Tijsseling, A. S., Laanearu, J., Annus, I., Koppel, T., Bergant, A., Vučković, S., Anderson, A., & van 't Westende, J. M. C. (2014). Experimental investigation on rapid filling of a large-scale pipeline. *Journal of Hydraulic Engineering*, *140*(11), Article 04014053. https://doi.org/10.1061/(ASCE)HY.1943-7900.0000914

Lopez Sola, E., Calviani, M., Aberle, O., Ahdida, C., Avigni, P., Battistin, M., Bianchi, L., Burger, S., Busom Descarrega, J., Canhoto Espadanal, J., Cano-Pleite, E., Casolino, M., Fraser, M. A., Gilardoni, S., Girod, S., Grenard, J.-L., Grenier, D., Guinchard, M., Hessler, C., ... Zuccalli, L. (2019). Beam impact tests of a prototype target for the beam dump facility at CERN: Experimental setup and preliminary analysis of the online results. *Physical Review Accelerators and Beams*, *22*(12), Article 123001. https://doi.org/10.1103/PhysRevAccelBeams.22.123001

Malekpour, A., Karney, B. W., & Nault, J. (2016). Physical understanding of sudden pressurization of pipe systems with entrapped air: Energy auditing approach. *Journal of Hydraulic Engineering*, *142*(2), Article 04015049. https://doi.org/10.1061/(ASCE)HY.1943-7900.0001067

Martins, N. M. C., Delgado, J. N., Ramos, H. M., & Covas, D. I. C. (2017). Maximum transient pressures in a rapidly filling pipeline with entrapped air using a CFD model. *Journal of Hydraulic Research*, *55*(4), 506–519. https://doi.org/10.1080/00221686.2016.1275046

Miano, A., Fiorillo, A., Salzano, A., Prota, A., & Jacobsson, R. (2020). The structural design of the decay volume for the search for hidden particles (SHIP) project. *Archives of Civil and Mechanical Engineering*, *21*(1), Article 3. https://doi.org/10.1007/s43452-020-00152-9

Minh, H.-L., Sang-To, T., Le-Van, B., Le-Tien, L., & Cuong-Le, T. (2024). Design optimization of a large industrial steel structure using an enhanced K-means clustering optimizer and finite-element model updating. *Archives of Civil and Mechanical Engineering*, *25*(1), Article 55. https://doi.org/10.1007/s43452-024-01092-4

Mittelstedt, C. (2023). *Theory of plates and shells*. Springer. https://doi.org/10.1007/978-3-662-66805-4

Rössing, F., Arutinov, D., Brignoli, A., Fischer, H., Grewing, C., Lacker, H., Lyons, F., Zambanini, A., & van Waasen, S. (2024). *Design space exploration for particle detector read-out implementations in Matlab and Simulink on the example of the SHiP SBT*. arXiv. https://doi.org/10.48550/arXiv.2402.03122

Svendsen, B. T., Petersen, Ø. W., Frøseth, G. T., & Rønnquist, A. (2023). Improved finite element model updating of a full-scale steel bridge using sensitivity analysis. *Structure and Infrastructure Engineering*, *19*(3), 315–331. https://doi.org/10.1080/15732479.2021.1944227

Tijsseling, A. S., Hou, Q., Bozkuş, Z., & Laanearu, J. (2016). Improved one-dimensional models for rapid emptying and filling of pipelines. *Journal of Pressure Vessel Technology*, *138*(3), Article 031301. https://doi.org/10.1115/1.4031508

Truong, D.-N., & Chou, J.-S. (2023). Integrating enhanced optimization with finite element analysis for designing steel structure weight under multiple constraints. *Journal of Civil Engineering and Management*, *29*(8), 757–786. https://doi.org/10.3846/jcem.2023.20399

Venskus, A., Kalanta, S., Atkočiūnas, J., & Ulitinas, T. (2010). Integrated load optimization of elastic–plastic axisymmetric plates at shakedown. *Journal of Civil Engineering and Management*, *16*(2), 203–208. https://doi.org/10.3846/jcem.2010.22

White, F. M. (2016). *Fluid mechanics* (8th ed.). McGraw-Hill Education.

Zhou, L., & Liu, D. (2013). Experimental investigation of entrapped air pocket in a partially full water pipe. *Journal of Hydraulic Research*, *51*(4), 469–474. https://doi.org/10.1080/00221686.2013.785985

Zhou, L., Liu, D., & Ou, C. (2011). Simulation of flow transients in a water filling pipe containing entrapped air pocket with VOF model. *Engineering Applications of Computational Fluid Mechanics*, *5*(1), 127–140. https://doi.org/10.1080/19942060.2011.11015357

Zhou, L., Wang, H., Karney, B., Liu, D., Wang, P., & Guo, S. (2018). Dynamic behavior of entrapped air pocket in a water filling pipeline. *Journal of Hydraulic Engineering*, *144*(8), Article 04018046. https://doi.org/10.1061/(ASCE)HY.1943-7900.0001491

Zingoni, A. (2017). Membrane theory of shells of revolution. In *Shell structures in civil and mechanical engineering* (Chapter 2, pp. 35–56). ICE Publishing. https://doi.org/10.1680/ssicame.60289.035